

ArtiBoost: Boosting Articulated 3D Hand-Object Pose Estimation via Online Exploration and Synthesis

Kailin Li^{*}, Lixin Yang^{*}, Xinyu Zhan, Jun Lv, Wenqiang Xu, Jiefeng Li, Cewu Lu[†]
Shanghai Jiao Tong University, China

{kailinli, siriusyang, kelvin34501, LyuJune.SJTU, vinjohn, ljf_likit, lucewu}@sjtu.edu.cn

Abstract

Estimating the articulated 3D hand-object pose from a single RGB image is a highly ambiguous and challenging problem requiring large-scale datasets that contain diverse hand poses, object poses, and camera viewpoints. Most real-world datasets lack this diversity. In contrast, synthetic datasets can easily ensure vast diversity, but learning from them is inefficient and suffers from heavy training consumption. To address the above issues, we propose ArtiBoost, a lightweight online data enrichment method that boosts articulated hand-object pose estimation from the data perspective. ArtiBoost is employed along with a real-world source dataset. During training, ArtiBoost alternatively performs data exploration and synthesis. ArtiBoost can cover various hand-object poses and camera viewpoints based on a Compositional hand-object Configuration and Viewpoint space (CCV-space) and can adaptively enrich the current hard-discernable samples by a mining strategy. We apply ArtiBoost on a simple learning baseline network and demonstrate the performance boost on several hand-object benchmarks. As an illustrative example, with ArtiBoost, even a simple baseline network can outperform the previous start-of-the-art based on Transformer on the HO3D dataset. Our code is available at <https://github.com/MVIG-SJTU/ArtiBoost>.

1. Introduction

Articulated bodies, such as the human hand, body, and linkage mechanism, can be observed every day in our life. As it has more degree of freedoms (DoFs), the most useful information about the articulated body is preserved in its configuration space (C-Space). Extracting the configuration from a single image, which is usually referred to as the “Pose Estimation” [24, 4, 25], can benefit many down-

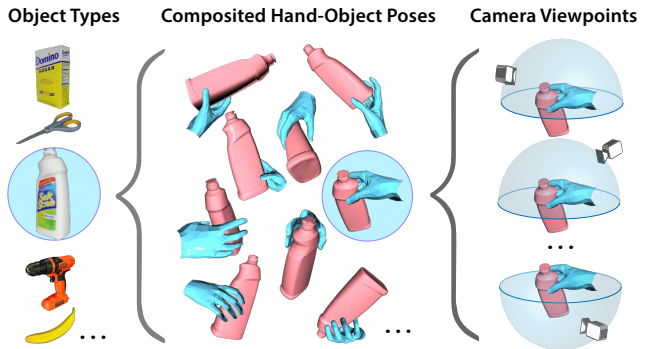


Figure 1. An intuitive illustration of the CCV-space.

stream tasks for human behavior understanding [5, 23]. Pose estimation for the articulated body is especially challenging owing to its high DoFs and projection ambiguity. Compositional pose estimation, which estimates the poses of multi-body articulation (e.g. hand-object interaction) is even more challenging as it suffers from severe self- or mutual occlusion. In this work, we are particularly interested in a certain type of compositional articulation – conjoint hand and object pose during interaction. The human hand has 16 joints and approximately 21 DoFs that is more than the most common articulated body, and conjoint hand-object pose estimation holds great potential for imitation learning.

As the dimension of C-Space grows, the proper amount of data to cover the configurations has grown exponentially. Preparing the training data for hand-object pose estimation (HOPE) can be very challenging. First, it is impractical to ask the subjects to systematically change their hand pose when interacting with object during recording. Second, different annotation approaches [1, 8, 13] may hinder the diversity unintentionally. For example, the multi-view-based approaches [1, 13] require the subject to maintain a predefined and static grasping pose in a video sequence. As a result, the efficiency of pose annotation with these approaches is considerably low. Meanwhile, previous works that explore the synthetic dataset have been repeatedly proven its efficacy to enhance the real data for training neural networks

^{*}The first two authors contribute equally.

[†]Cewu Lu is the corresponding author. He is the member of Qing Yuan Research Institute and MoE Key Lab of Artificial Intelligence, AI Institute, Shanghai Jiao Tong University, China.

[18, 50], as synthetic data can easily cover diverse configurations and viewpoints. The data synthesizing phase of these works was separated from the training phase, referred to as offline enrichment. However, not every hand-object configuration is helpful for training the HOPE model. For example, similar configurations may have already been observed multiple times, and those easily discernable samples may have a frequent appearance. Hence, offline enrichment, without repeatedly interacting with the model during training, is considered inefficient for the HOPE task.

To address the above issues, we propose an online data enrichment method, named **ArtiBoost**, to effectively **boost** the **articulated** hand-object pose estimation via two alternative steps during training, namely exploration and synthesis. At the exploration step, ArtiBoost explores a proposed Compositional hand-object Configuration and camera Viewpoint space (denoted as CCV-space) and samples triplets of the hand-object-viewpoint pose from it. Then at the synthesis stage, the polygon meshes of the sampled hand and object in the sampled viewpoint direction are rendered to the RGB images with photorealistic texture. The synthetic images are mixed with the real-world source images in batches to train a HOPE model. Later, the training losses are treated as feedback to guide the exploration step to mine the current hard-discernable samples for the next round of training. With such interaction in the training loop, ArtiBoost learns to adjust its sampling weights to customize more hardly-discernable data for the current HOPE model. As the HOPE model becomes powerful, it can also continuously promote the current ArtiBoost to evolve.

At the exploration stage, we discretize the observation of arbitrary hand-object interaction in a proposed CCV-space which contains the dimension of object types, hand poses, and viewpoint directions. Furthermore, we define a contact-guided optimization method for generating valid and versatile hand-object interactions to enhance the source dataset during the training process. At the synthesis stage, ArtiBoost can support online rendering of the photorealistic hand and object mesh models onto a 224×224 canvas at 120 fps per graphic card (Titan X), far exceeding the expected speed for training. ArtiBoost is model-agnostic, which means that it can be plugged into any modern CNN architecture. As ArtiBoost directly enriches image data, both ArtiBoost and HOPE model are jointly trained in an end-to-end manner from scratch.

At the evaluation, we report the performance on three challenging HOPE benchmarks: FHAB [8], HO3D [13] and DexYCB [3]. To note, while ArtiBoost can be plugged into any sophisticated learning framework, we adopt a simple classification-based [40] and regression-based [16] baseline model to demonstrate its effectiveness. Without whistles and bells, the simple model can outperform the results of state-of-the-art (SOTA). Our contributions are summarized

in threefold:

- We propose the ArtiBoost. To the best of our knowledge, it is the first online data enrichment method for articulated hand-object pose estimation.
- Inside ArtiBoost, we propose a CCV-space that contains large-scale interacting poses and viewing directions. To generate such poses, we propose a contact-guided optimization that can ensure flexible and versatile interactions of hands and objects.
- Based on CCV-space, we introduce a weight-guided exploration strategy that can enrich data diversity and enlarge sample difficulty in the meantime. By adopting ArtiBoost, even a simple learning framework can outperform the state-of-the-art on various 3D hand-object benchmarks.

2. Related Work

Hand-Object Pose Estimation. As some HOPE tasks are closely related to hand pose estimation (HPE) tasks, we firstly walk through several HPE methods. According to its output form, single RGB-based 3D HPE can be categorized into three types: image-to-pose (I2P) [45], image-to-geometry (I2G) [4, 42], and hybrid [48]. While the I2P only focuses on the joints' pose themselves, the I2G focus on recover the full hand geometry (as mesh). Meanwhile, recent works [48, 44, 24] showed that I2G can be hybridized to I2P through neural inverse kinematics (IK). Second, we explore several HOPE methods. Regarding the learning-based methods, some aimed to predict the hand-object poses in a unified model [16, 29], while the others focused on recovering hand-object interaction based on contact modeling [46, 11]. As for the learning-free methods, Hasson *et al.* [17] and Cao *et al.* [2] proposed to aggregate the visual cues from object detection, HPE, and instance segmentation to acquire the optimal hand-object configuration.

This paper adopts a simple learning baseline network in two paradigms (classification and regression-based) for the HOPE task. We show that with ArtiBoost, even simple baseline networks can outperform several sophisticated designs.

Data Synthesis for Hand-Object Pose Estimation. Data synthesis in HOPE task includes two aspects, namely image and pose synthesis. In terms of image synthesis, ObMan [18] leveraged virtual avatars that pose grasping hand in a simulator and rendered images through virtual cameras. ContactPose [1] synthesized images through real hand and background composition. In terms of pose synthesis, there are also two genres included in literature. The metric-based methods [18, 6] leveraged grasping software [33] to simulate hand poses subjected to physical grasping metrics.

The data-driven methods [41, 22] utilize the hand-object datasets to learn conditional VAE that generates new poses.

This paper presents a novel contact-guided optimization method in CCV-space to construct more diverse poses of hand-object interaction.

Exploration for Hard Examples, also called “hard example/negative mining”, has been proven effective for various computer vision tasks, such as object detection [27, 38], person re-id [20], face recognition [37], and deep metric learning [9, 39]. Generally speaking, the basic ideology of hard examples mining is that if a prediction of a certain data sample exhibits a large error under a certain metric, then this data sample is not properly learned by the learning algorithm. By adding such data samples to the training batch can help the learning converge faster. Recent work also exploited a learnable generation model [10] to acquire harder unseen samples based on error feedback training. However, it must pay non-trivial efforts on the adversarial part to acquire valid samples.

In this paper, as the proposed CCV-space already ensures poses’ diversity and validity, we adopt a simple yet effective online mining strategy for hard-discernable hand-object-viewpoint triplets, which has not been done in the previous works.

3. Method

3.1. Overview

This section describes the exploration and synthesis step in ArtiBoost and elaborates the learning framework for the HOPE task. Inside the explorations step, we present the compositional configurations and viewpoints space (CCV-space), the key component of ArtiBoost.

Problem Definition. Given an input image $\mathbf{I} \in \mathbb{R}^{H \times W \times 3}$ that observes a single hand interacting with a certain object, HOPE aims to learn a certain neural network that predict the 3D hand joint locations: $\mathbf{P}_h = \{\mathbf{p}_j\}_{j=1}^J$, object centroid locations: \mathbf{p}_o and object rotation: $\mathbf{r}_o \in \mathfrak{so}(3)$, where $\mathbf{p}_j, \mathbf{p}_o \in \mathbb{R}^3$, $J = 21$ and the $H \times W$ is the resolution.

To train the neural network, we shall firstly prepare a real-world source dataset: \mathcal{D}_{real} . ArtiBoost is employed along with the \mathcal{D}_{real} . During the training process, ArtiBoost iteratively samples (without replacement) hand-object-viewpoint triplets from the CCV-space: \mathcal{C} based on a weight map: \mathbf{M} . Each entry of \mathbf{M} corresponds to a certain triplet in \mathcal{C} , and the value in that entry corresponds to the sampling weight of the triplet. Meanwhile, those selected triplets are rendered as a batch of synthetic images at the synthesis step. The synthetic images are mixed with source images from \mathcal{D}_{real} . After that, the mixed batch is fed to the HOPE learning framework to complete a forward and backward propagation. When an epoch of training has finished,

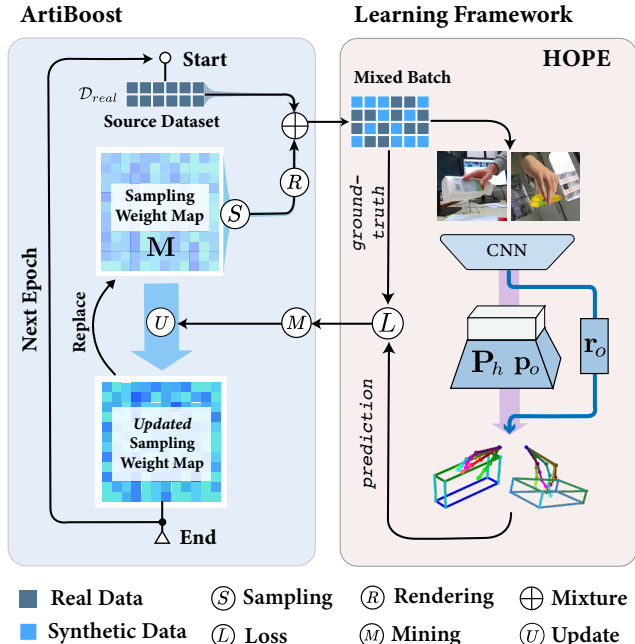


Figure 2. **Illustration of the integrated pipeline.** ArtiBoost can be plugged into an arbitrary HOPE framework by simply modifying the current data loader.

ArtiBoost updates the sampling weights in \mathbf{M} based on the mining result in its exploration step and waits for the next round of training. The whole pipeline is illustrated in Fig 2.

3.2. Online Exploration in CCV-Space

The Compositional Configuration & Viewpoint Space. HOPE problem commonly involves a certain interacting hand-object configuration that is observed by a certain viewpoint. The input domain of HPE can thus be narrowed down to three main dimensions: object type, hand pose, and viewpoint direction. To note, the dimension of object type and hand pose are not independent of each other. Given a certain object model, the hand pose that interacts with it depends on the local geometry of the model. As shown in Fig 1, we define the discrete representation of the input domain as the CCV-space: $\mathcal{S} = \{(n_o, n_p, n_v) \in \mathbb{N}_+^3 \mid n_o \leq N_o, n_p \leq N_p, n_v \leq N_v\}$, where the N_o, N_p and N_v is the number of object types, discrete poses and viewpoints, respectively. The (i, j, k) item in \mathcal{S} stands for the scenario that the interaction between the i -th object and the j -th hand pose is observed at the k -th camera viewpoint. Next, we will sequentially present the components in CCV-space, namely: hand configuration space (**C-space**), composited hand-object configuration space (**CC-space**) and viewpoint space (**V-space**).

C-Space of Valid Hand Pose. To represent hand, we employ a parametric skinning hand model, MANO [36] which

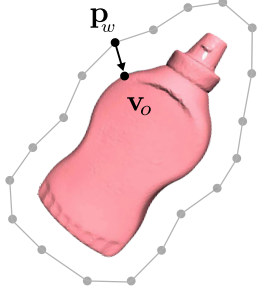


Figure 3. Offset surface.

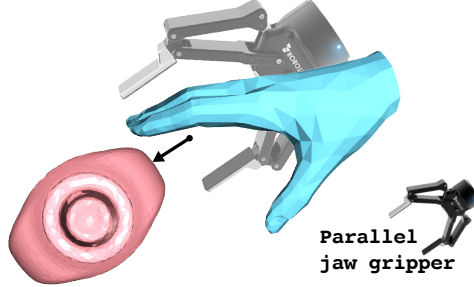


Figure 4. Pre-grasping hand pose.

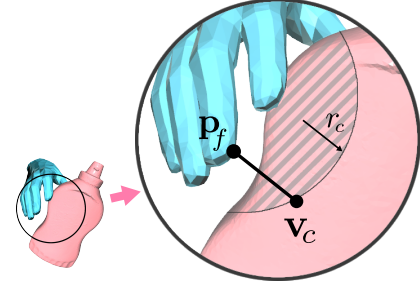


Figure 5. Fingertip and its contact point.

drives an articulated hand mesh with 16 joints rotations $\theta \in \mathbb{R}^{16 \times 3}$ and shape parameters $\beta \in \mathbb{R}^{10}$. Given the axis-angle forms of rotation, MANO has 48 DoFs that exceed the DoFs allowed by a valid hand pose [26]. Fitting or interpolation on the 48 DoFs rotations may encounter abnormal hand pose that is unhealthy for training the HOPE network. Besides, the original MANO’s coordinate system is not coaxial with the direction of the hand’s kinematic tree, so that the rotation axis is coupled with at least two of the MANO’s orthogonal axes. This property makes the pose interpolation more difficult. In the paper, we employ an axis adaptation based on the *twist-splay-bend* coordinate system that was initially proposed by [46]. It enables us to describe the hand pose at each joint as the rotation angle along with one of the specified coordinate axis (*e.g. bend*) at this joint. With the axis adaptation, we design three protocols for describing the C-space of valid hand pose:

- i). According to hand anatomy, all the non-metacarpal joints along the hand’s kinematic tree can only have the bending pose. And the five metacarpal joints can only have a combined bending and splaying poses. Any twisting along the pointing direction or splaying at non-metacarpal joints is prohibited.
- ii). For each of the five fingers, the bending poses on their proximal and distal joint are linked and dependent. The bending poses at the five metacarpal joints are independent of other joints.
- iii). The pose of each finger is independent of each other as long as it does not conflict with the protocol i) & ii).

Based on these protocols, the total DoFs in the hand’s C-space is 21 (one splaying and two independent bending DoFs for each of the five fingers, plus 6 DoFs at the wrist). Hence, we can describe the whole hand pose by describing the angles of 15 joints’ rotation along its specified axis: θ_i^{bend} or θ_i^{splay} , as well as the wrist pose: $\xi_w \in \mathfrak{se}(3)$. These protocols not only guarantee the diversity and validness of hand pose but also ensure the poses are visually plausible for vision tasks. After ensuring a valid C-space, we now

move on to the composited space that describes hand-object interaction.

Composited C-space of Hand-Object Interaction. We firstly define the hand-object “interaction” as the scenario that satisfies the following requirements: **i)** The thumb and at least one or more fingers should be in contact with the object surface [41]; **ii)** The hand and object model should not intersecting with each other; As the hand’s interacting pose is highly dependent on the object model’s approaching direction and local geometry, only a tiny portion of poses in hand C-space is valid for interaction purposes. Hence instead of searching for valid interaction poses in the entire hand C-space, we turn to explore a discrete space of pre-defined hand-object poses. We call it Composited C-space (CC-space).

To construct the CC-space, we need to generate considerable amounts of hand-object poses. However, this process is not easy. Previous methods based on the off-the-shelf grasping simulator [18, 6] lack the diversity and flexibility on hand poses. For example, the amount of different poses per object in GanHand [6] does not exceed 12. Previous datasets [1, 41] capturing real-world hand-object interaction also lack this diversity: there are only a few distinct hand-object poses in a full video sequence. The goal of CC-space is to enlarge the diversity of interactive hand poses for a given object. We propose a fitting-based pose generation method to this end. This method is divided into three steps.

1). First, given an object model, we construct an offset surface outside of its original surface and uniformly sample N_w points on the offset surface (Fig 3). These points will control the wrist position. For each point: \mathbf{p}_w , we query its closet vertex on object surface: \mathbf{v}_o . The vector: $\mathbf{v}_o - \mathbf{p}_w$ stands for the approaching direction of hand to object. Then, we construct a pre-grasping hand model that mimics the pose of a parallel jaw gripper (Fig 4). This pre-grasping hand is placed at each \mathbf{p}_w as interaction initiation. The \mathbf{p}_w ’s approaching direction controls the movement of the wrist. Based on a certain \mathbf{p}_w , we define the region between \mathbf{v}_o and the farthest vertex that the finger can reach as the object’s contact-feasible region.

2). Second, to generate the interacting pose, we fit the fingertips to contact point \mathbf{v}_c chosen from contact-feasible region (Fig 5). For each \mathbf{p}_w , we generate N_p^w interacting hand poses. To increase diversity, we employ several randomness during fitting: **i)** We randomly select thumb and N ($1 \leq N \leq 4$) other fingers on hand. Only the selected fingers will participate in fitting. **ii)** For each selected fingers, we set a random minimal reaching radius r_c inside the contact-feasible region. Now the selected fingertip must reach for a contact point \mathbf{v}_c that satisfies: **i)** $\|\mathbf{v}_c - \mathbf{p}_w\|_2 \geq r_c$; **ii)** $\min_{\mathbf{v}_c} \|\mathbf{v}_c - \mathbf{p}_f\|_2$, where the \mathbf{p}_f is the selected fingertip point. After each selected fingertip is paired with a certain contact point, we will initiate the fitting process.

3). During fitting, we adopt the anchor-based hand model and contact-based energy function defined by [46]. The fitting process aims to minimize the energy brought from unattached fingertips and contact points: the unattached anchor on a fingertip: \mathbf{p}_f will be attracted to its corresponded contact point \mathbf{v}_c on the object, while the intersected anchors will be pushed out. The fitting of hand poses is only performed on the predefined DoFs in the hand’s C-space. Thus the validness of hand poses can be guaranteed.

Viewpoint Space. For the camera viewpoint, we uniformly sample N_v viewpoints direction \mathbf{n}_v according to the sphere sampling strategy [31]:

$$\mathbf{n}_v = (\sqrt{1 - u^2} \cos(\phi), \sqrt{1 - u^2} \sin(\phi), u)^\top \quad (1)$$

where $u \sim \mathcal{U}[-1, 1]$ and $\phi \sim \mathcal{U}[0, 2\pi]$, where \mathcal{U} stands for uniform distribution.

Weight-Guided Sampling Strategy. In literature, the uniform sampling strategy was widely adopted by synthetic dataset [49, 18, 34]. However, not every sample in the CV-space contributes equally to the network. Since we hope that those hardly discernable samples shall have a higher frequency of occurrence, we construct a weight map $\mathbf{M} \in \mathbb{R}^{N_o \times N_p \times N_v}$ to guide the sampling in the exploration step. In \mathbf{M} , each element w_i stands for the sampling weight of the corresponding item in CV-space. The probability p_i of a certain item that would be sampled is $p_i = w_i / \sum w_j$. We then draws N_{syn} samples from the multinomial distribution $\{p_i \mid p_i = w_i / \sum w_j; w_i, w_j \in \mathbf{M}\}$. Based on this strategy, we shall increase the weights for those hardly discernable samples in \mathbf{M} while decreasing the weights for those who are already easy to discern, when we get the feedback from the mining results.

Mining Strategy. After an epoch of training has finished, ArtiBoost mines those hardly discernable items and marks them as the ‘hard examples’. In this paper, we inspect a percentile-based mining strategy. During the mining phase, each synthetic sample will be assigned a weight update. These updates are multiplied by the original sampling

weight in \mathbf{M} . Intuitively, we want those hardly discernable samples to have high weight. In the percentile-based mining strategy, we calculate the weight update based on the percentile of the samples’ Mean Per Joint Position Error (MPJPE) among the whole epoch of synthetic samples. For the i -th sample, given by the MPJPE e_i and its percentile $q_i = \frac{e_{\max} - e_i}{e_{\max} - e_{\min}}$, the weight update are calculated from a simple reciprocal heuristic: $\delta w_i = \frac{1}{q_i + 0.5}$. If the sample i has the maximum MPJPE e_{\max} among the synthetic samples in current epoch, its original sampling weight in \mathbf{M} will be multiplied by a maximum update factor $\delta w_i = 2$. If the i has the minimum MPJPE e_{\min} , its update factor would be $\delta w_i = 2/3$. We also clamp the updated \mathbf{M} by a upper bound 2.0 and lower bound 0.1 to avoid over imbalance.

3.3. Online Synthesis for HOPE task

During the training process, we synthesize the sampled hand-object-viewpoint triplets to RGB images. This synthesis process is task-oriented, as the adaptive sampling decides its composition to cater to the downstream task. Here, we describe the features in the online synthesis step.

Disturbance on the Triplets. Given an object, if only the discrete N_p poses and N_v viewpoints in the CCV-space would appear, the HOPE model is prone to overfitting. To improve the generalization ability, we also add disturbance on the hand poses and viewpoint directions before rendering images.

- *For the hand poses*, we relieve the restriction on protocol **ii)** in hand C-space, in which the bending angles of distal and proximal joints on each finger are now independent in terms of disturbance. Then, we add a Gaussian disturbance $\mathcal{N}(0, \sigma_1^2)$ on each of the 15 bending angles. Second, for the disturbance on splaying angles, we add a $\mathcal{N}(0, \sigma_2^2)$ on the five metacarpal joints. We empirically set $\sigma_1 = 3$ and $\sigma_2 = 1.5$ degree. However, disturbance on hand poses may cause the intersection between the hand and object. We borrow the RefineNet model [41] to mitigate such phenomenon.

- *For the viewpoint directions*, we add three disturbances: $\mathcal{U}(-\delta u, +\delta u)$, $\mathcal{U}(-\delta \phi, +\delta \phi)$, and $\mathcal{U}(0, 2\pi)$ on the elevation distance u , azimuth angle ϕ and the camera in-plane rotation, respectively. In all experiments, we empirically set $\delta u = 0.05$ and $\delta \phi = 7.5$ degree.

Skin Tone & Textures. We adopt a state-of-the-art hand skin tone & texture model: HTML [35] for realistic appearance on the rendered images. HTML represents the hand’s skin color & texture of as continuous parameters in a PCA space. Before the refined hand model enters the rendering pipeline, we randomly assign it an HTML texture map. We empirically discard the shadow removal operation in HTML, which results in more visually plausible images.



Figure 6. The rendered images during online synthesis.

Rendering. We employ the off-the-shelf rendering software: Pyrender [32] inside ArtiBoost. The interactive hand and object are the foreground, and the images in COCO [28] dataset are the background. The canvas size is set as 244×244 in all experiments. The synthesized data is the combination of four task-oriented items, namely hand-object-viewpoint triplet, background, skin tone and texture. We show several rendered images in Fig 6.

3.4. Learning Framework

We adopt two simple baseline network: one is classification-based (*Clas*) and the other regression-based (*Reg*). We employ ResNet-34 [19] as the backbone in both of them. In *Clas*, we use two de-convolution layers to generate 22 3D-heatmaps that indicate the location of 22 joints (21 hand joints and one object centroid) as likelihood. The 22 3D-heatmaps are defined in a restricted uvd space, where uv is the pixel coordinates, and d is the a wrist-relative depth value. Then, we employ a soft-argmax operator to convert the 3D-heatmaps into joints’ uvd coordinates. Finally, we transform the joints’ uvd coordinates into its 3D locations: $\mathbf{P}_h, \mathbf{p}_o$ in camera space by camera intrinsic: \mathbf{K} and wrist location: \mathbf{p}_w . In *Reg*, we use multi-layer perceptron (MLP) to regress the MANO parameters: θ, β and object centroid: ${}^w\mathbf{p}_o$ w.r.t. the wrist. Then we transfer the θ, β to the wrist-relative hand joints: ${}^w\mathbf{P}_h$ by the MANO model. Finally the ${}^w\mathbf{P}_h$ and ${}^w\mathbf{p}_o$ are translated into the camera space by adding a known wrist location: \mathbf{p}_w . Both *Clas* and *Reg* adopt another MLP branch to predict the object rotation: \mathbf{r}_o .

Loss Function. The loss function to train the HOPE network consists of four terms.

First, we penalize the error of total 22 joints location (21 hand joints and 1 object centroid) in form of ℓ_2 distance:

$$\mathcal{L}_{loc} = \frac{1}{22} \sum_{i=1}^{22} \left\| \mathbf{p}_i - \hat{\mathbf{p}}_i \right\|_2^2 \quad (2)$$

where $\hat{\mathbf{p}}_i$ denotes the ground-truth joint location.

Second, we penalize the error of object rotation in form of ℓ_2 distance at the eight tightest bounding box corners:

$$\mathcal{L}_{cor} = \frac{1}{8} \sum_{i=1}^8 \left\| \exp(\mathbf{r}_o) * \bar{\mathbf{c}}_i - \hat{\mathbf{c}}_i \right\|_2^2 \quad (3)$$

where the $\bar{\mathbf{c}}_i$ and $\hat{\mathbf{c}}_i$ are the object’s corners in canonical

view and camera view. $\exp(\mathbf{r}_o)$ is the predicted rotation matrix.

Third, we adopt the ordinal relation loss to correct the 2D-3D misalignment. \mathcal{L}_{ord} inspects the joint-level depth relation inside a pair of joints: one from the 21 hand joints and the other from the 8 object corners. We penalize the case if the predicted depth relation between the i -th hand joint: \mathbf{p}_i and the j -th corner \mathbf{c}_j is misaligned with its ground-truth relation: $\mathbb{1}_{i,j}^{ord}$. The \mathcal{L}_{ord} is formulated as:

$$\mathcal{L}_{ord} = \sum_{j=1}^8 \sum_{i=1}^{J=21} \mathbb{1}_{i,j}^{ord} * \left| (\mathbf{p}_i - \mathbf{c}_j) \cdot \mathbf{n}_\perp \right| \quad (4)$$

where the \mathbf{n}_\perp is the viewpoint direction.

Fourth, we borrow a symmetry-aware object corner loss: \mathcal{L}_{sym} from Hampali *et al.* [15]:

$$\mathcal{L}_{sym} = \min_{\mathbf{R} \in \mathcal{S}} \frac{1}{8} \sum_{i=1}^8 \left\| \exp(\mathbf{r}_o) * \bar{\mathbf{c}}_i - \exp(\hat{\mathbf{r}}_o) \mathbf{R} * \bar{\mathbf{c}}_i \right\|_2^2 \quad (5)$$

where $\exp(\hat{\mathbf{r}}_o)$ denotes object’s ground-truth rotation matrix. Given an object, the set \mathcal{S} contains all the valid rotation matrices based on the object’s predefined symmetry axes.

The overall loss is a weighted sum of the four terms:

$$\mathcal{L}_{HOPE} = \mathcal{L}_{loc} + \lambda_1 \mathcal{L}_{cor} + \lambda_2 \mathcal{L}_{ord} + \lambda_3 \mathcal{L}_{sym} \quad (6)$$

where the $\lambda_{1 \sim 3}$ are the hyper-parameters.

4. Evaluation and Result

4.1. Dataset and Metrics

Dataset. We evaluate our methods on three hand-object dataset: **FHAB** [8], **HO3D** [13] and **DexYCB** [3]. FHAB contains 20K samples of hand in manipulation with objects. We follow the “action” split as in Tekin *et al.* [43], which contains 10,503 training and 10,998 testing samples. The FHAB dataset only contains a few numbers of hand poses and viewpoints, and we find its training set is adequate for the neural network. Thus we only use FHAB to verify the feasibility of the learning framework. HO3D is a dataset that contains a large number of images of hand-object interactions. Evaluation of the HO3D testing set is conducted at an online server. We also report our results on the latest **HO3D v3** [14], which is released with different training/testing split. DexYCB contains 582K image frames of grasping on 20 YCB objects. We only evaluate the right-hand pose using the official “S0” split and filter out the frames that the minimum hand-object distance is large than 5 *cm*.

Metrics. For the hand pose, we report the mean per joint position error (**MPJPE**) in the wrist-aligned coordinates

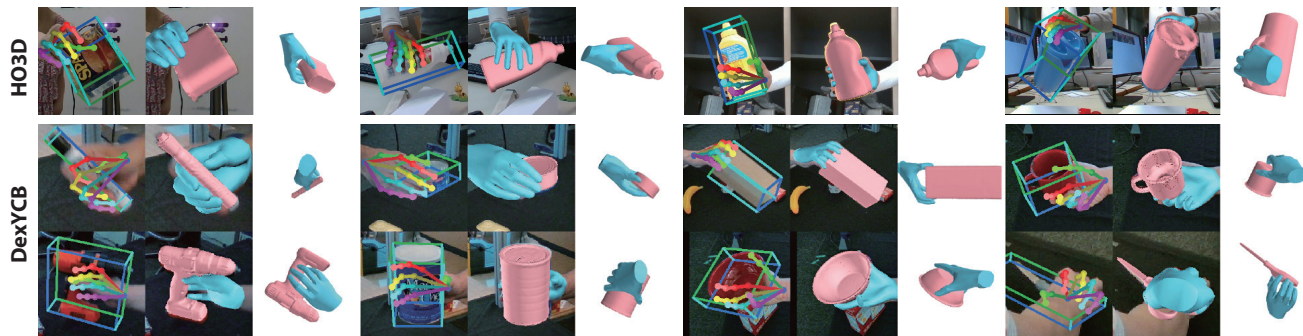


Figure 7. (Best view in color) Qualitative results on the HO3D (1st row) and DexYCB dataset (2nd, 3rd rows).

system. For the object pose, there are two standard metrics in literature: mean per corners position error (**MPCPE**) and maximum symmetry-aware surface distance (**MSSD**). The former MPCPE directly measures the unique pose of the object. However, since some objects are symmetrical or revolutionary invariant by nature, and since the objects are often severely occluded by hand, direct measuring object’s absolute and unique pose is sometimes less reasonable. MSSD measures the difference between the current object pose to its closest counterpart in all its rotation invariants. In this paper, we report the object’s MPCPE and MSSD within different training schemes. When reporting MPCPE, we train the network with $\lambda_1 = \lambda_2 = 1$ and $\lambda_3 = 0$. When taking objects’ symmetry into account, we train the network with $\lambda_1 = \lambda_2 = 0$ and $\lambda_3 = 1$. We call the later network symmetry model (abbr. sym) and report its MSSD following the BOP challenge protocol [21]. The definition of YCB objects’ symmetry axes can be found in the supplementary material.

4.2. Implementation Details

The CCV-space. In the composited C-space, we fit 300 different interacting poses for each object. As the optimization may result in local minima, we manually discard the poses that **i)** exhibit severe inter-penetration between hand and object; **ii)** form an unnatural grasping or interaction. As a result, the total interacting hand poses per object N_p is roughly 100. In the viewpoints space, we choose $N_u = 12$ and $N_\phi = 24$, which comprise $N_v = N_u \times N_\phi = 288$ different viewpoints in total. Thus, the total number of different hand-object-viewpoint triplets in *e.g.* DexYCB dataset is: $N_o \times N_p \times N_v = 20$ (# of objects) $\times 100 \times 288 = 576,000$.

The Training Details. We use ResNet-34 as the backbone in both classification-based (*Clas*) and regression-based (*Reg*) baseline networks. The backbone is initialized with ImageNet [7] pretrained model. In *Clas*, the output res-

olution of 3D-heatmaps is $28 \times 28 \times 28$. The MLP branch that predicts object rotation adopts three fully-connected layers with 512, 256 and 128 neurons for each, and a final layer of 6 neurons that predict the continuity representation [47] of object rotation: $\mathbf{r}_o \in \mathfrak{so}(3)$. We train the network 100 epochs. We use Adam optimizer and set the learning rate to 5×10^{-5} . We train our ArtiBoost with a mini-batch size of 64 per GPU and 2 GPUs in total. The framework is implemented in PyTorch.

4.3. HOPE Network Performance

Qualitative Results. Our qualitative results on HO3D and DexYCB testing sets are showed in Fig 7. We draw the predicted hand joints and object corners as projections on 2D image (1st column). We also adopt a pretrained IK network [30] that converts the hand joints’ location to hand geometry for visualization. We draw the full hand-object geometry in camera view (2nd column) and other viewpoint (3rd column).

Comparison with State-of-the-Art. In Tab 1 we compare our *Clas* with the previous SOTA on FHAB to justify the ordinal relation loss \mathcal{L}_{ord} . To note, [16] regressed hand and object poses in camera space. For fair comparison, we align their results in wrist-relative coordinates system. In Tab 2, we show that our ArtiBoost (abbr. Arti) enhances both *Reg* and *Clas* performance on HO3D dataset. We obtain **28%** and **10%** MPJPE improvement compared with the previous SOTA [16] and [29], respectively. For fair comparison, we remove the unseen object (*pitcher base*) when calculating MPCPE.

Under the symmetry model, we report the performance of our ArtiBoost in Tab 3. Our *Clas* even outperforms the recent Transformer-based method [15] when using ArtiBoost. We also evaluate our method on latest released dataset DexYCB and HO3D v3 in Tab 4 and Tab 5, respectively. Both results demonstrate the effectiveness of our method.

| Method | MPJPE | MPCPE |
|---|-------------|--------------|
| Hasson <i>et al.</i> [16] | 11.33 | 28.42 |
| Our <i>Clas</i> w/o \mathcal{L}_{ord} | 8.71 | 18.64 |
| Our <i>Clas</i> | 8.60 | 19.45 |

Table 1. Comparisons with SOTA on **FHAB** dataset (errors are reported in *mm*). The comparisons are made in the wrist-aligned coordinates system.

| Method | MPJPE | MPCPE |
|-------------------------------|-------------|-------------|
| Hasson <i>et al.</i> [16] | 3.69 | 12.38 |
| Liu <i>et al.</i> [29] | 2.93 | - |
| Our <i>Reg</i> | 3.53 | 7.38 |
| Our <i>Reg</i> + Arti | 3.17 | 5.87 |
| Our <i>Clas</i> | 3.06 | 7.24 |
| Our <i>Clas</i> + Arti | 2.64 | 5.16 |

Table 2. Comparisons (*cm*) with SOTA on **HO3D** dataset.

| Method | MPJPE | MSSD | | |
|-----------------------------------|-------------|---------------------------------|----------------------------------|----------------------------------|
| | | <i>mustard</i> <i>bottle</i> | <i>bleach</i> <i>cleanser</i> | <i>potted</i> <i>meat can</i> |
| Hampali <i>et al.</i> [15] | 2.57 | 4.41 | 6.03 | 9.08 |
| Our <i>Clas</i> sym | 3.10 | 4.07 | 6.56 | 8.70 |
| Our <i>Clas</i> sym + Arti | 2.53 | 3.14 | 5.72 | 6.36 |

Table 3. Comparison (*cm*) with Transformer-based SOTA on **HO3D** using symmetry-aware loss \mathcal{L}_{sym} . We use the same symmetry axes as in [15].

| Method | MPJPE | MSSD * | | | |
|-----------------------------------|--------------|------------------------------|------------------------------|-----------------|----------------------------------|
| | | <i>power</i> <i>drill</i> | <i>cracker</i> <i>box</i> | <i>scissors</i> | <i>bleach</i> <i>cleanser</i> |
| Our <i>Clas</i> sym | 13.00 | 74.95 | 63.68 | 88.10 | 91.66 |
| Our <i>Clas</i> sym + Arti | 12.80 | 52.70 | 46.13 | 66.52 | 72.31 |

Table 4. Our results (*mm*) on **DexYCB**. “*”: We only list the MSSD score of 4 objects. The full table can be found in supplementary material.

| Method | MPJPE | MPCPE | MSSD | | |
|-----------------------------------|-------------|-------|---------------------------------|----------------------------------|----------------------------------|
| | | | <i>mustard</i> <i>bottle</i> | <i>bleach</i> <i>cleanser</i> | <i>potted</i> <i>meat can</i> |
| Our <i>Clas</i> | 2.94 | 7.53 | 6.88 | 5.56 | 7.63 |
| Our <i>Clas</i> + Arti | 2.50 | 5.88 | 3.79 | 4.99 | 6.21 |
| Our <i>Clas</i> sym | 2.98 | - | 3.73 | 6.39 | 7.28 |
| Our <i>Clas</i> sym + Arti | 2.34 | - | 2.66 | 5.23 | 5.82 |

Table 5. Our results (*cm*) on **HO3D v3**.

4.4. Ablation Study

Potential of Training on Less Labeled Data. In this study, we delve into discovering the potential of ArtiBoost on training with less amount of real-world labeled data. We train our framework using only a small portion of the HO3D dataset. As shown in Tab 6, we find that ArtiBoost can outperform the network trained with 100% real-world data even using 10 % of training samples.

| Method on % of source data | MPJPE | MPCPE |
|-------------------------------------|-------------|-------------|
| Our <i>Reg</i> (10%) | 3.81 | 8.77 |
| Our <i>Reg</i> (100%) | 3.53 | 7.38 |
| Our <i>Reg</i> (10%) + Arti | 3.29 | 6.87 |
| Our <i>Clas</i> (10%) | 3.63 | 7.66 |
| Our <i>Clas</i> (100%) | 3.06 | 7.24 |
| Our <i>Clas</i> (10%) + Arti | 3.05 | 6.02 |

Table 6. Results (*cm*) of *Reg* and *Clas* using 10% of **HO3D** source training data.

Portability of ArtiBoost. Our ArtiBoost, as a model-agnostic data enrichment method, can easily be ported to different learning frameworks. In Tab 7, we provide the results of porting ArtiBoost to another HOPE framework proposed by Hasson *et al.* [16]. The source training dataset: **HO3D v1** [12] used in [16] is an early version of HO3D

with “MC2” as the unique test sequence. We reproduced the results in [16] by training their network on the public v1 set only. As [16] directly regressed the hand joints and object poses in camera space, we also report the MPJPE in camera space for fair comparisons. We show in Tab 7 that adding ArtiBoost into [16] achieves a significant improvement on all metrics.

| Dataset | Method | MPJPE | MPCPE | CS-J |
|---------|---|-------------|-------------|-------------|
| HO3D v1 | Hasson <i>et al.</i> [16] | 5.75 | 9.61 | 6.24 |
| HO3D v1 | Hasson <i>et al.</i> [16] + Arti | 3.67 | 3.24 | 3.57 |
| HO3D | Hasson <i>et al.</i> [16] | 3.69 | 12.38 | 5.52 |
| HO3D | Hasson <i>et al.</i> [16] + Arti | 3.39 | 8.31 | 4.90 |

Table 7. Results of porting ArtiBoost to the frameworks in Hasson *et al.* [16]. CS-J denotes the MPJPE in camera space; all in *cm*.

Efficacy of Mining Strategy. In Tab 8, we demonstrate the effectiveness of the mining strategy. We inspect two experiments throughout the entire training process, one of which used the mining strategy and the other only used random sampling. We report their temporary results at a certain interval. Compared with the training without mining, our methods can achieve a higher score in a shorter period.

| Method | Interval (# of Epochs) | | | | |
|--|------------------------|--------------|--------------|--------------|--------------|
| | 20 | 40 | 60 | 80 | End |
| Our <i>Clas</i> sym + Arti w/o mining | 13.98 | 13.25 | 13.17 | 13.06 | 12.95 |
| Our <i>Clas</i> sym + Arti | 13.59 | 13.17 | 13.03 | 13.01 | 12.80 |

Table 8. Ablation study on mining strategy. We report the **MPJPE** (*mm*) on **DexYCB** dataset.

5. Conclusion

In this work, we propose a novel online data enrichment method ArtiBoost, which enhances the learning framework of articulated pose estimation by exploration and synthesis. Our proposed ArtiBoost can be integrated into any learning framework, and in this work, we show its efficacy on the challenging task of hand-object pose estimation. Even with a simple baseline, our method can boost it to outperform the previous SOTA on the popular datasets. Besides, the proposed CCV-space also open the door towards the generic articulated pose estimation, which we leave as future work.

References

- [1] Samarth Brahmabhatt, Chengcheng Tang, Christopher D Twigg, Charles C Kemp, and James Hays. ContactPose: A dataset of grasps with object contact and hand pose. In *ECCV*, 2020. 1, 2, 4
- [2] Zhe Cao, Ilija Radosavovic, Angjoo Kanazawa, and Jitendra Malik. Reconstructing hand-object interactions in the wild. In *ICCV*, 2021. 2
- [3] Yu-Wei Chao, Wei Yang, Yu Xiang, Pavlo Molchanov, Ankur Handa, Jonathan Tremblay, Yashraj S. Narang, Karl Van Wyk, Umar Iqbal, Stan Birchfield, Jan Kautz, and Dieter Fox. DexYCB: A benchmark for capturing hand grasping of objects. In *CVPR*, 2021. 2, 6
- [4] Xingyu Chen, Yufeng Liu, Chongyang Ma, Jianlong Chang, Huayan Wang, Tian Chen, Xiaoyan Guo, Pengfei Wan, and Wen Zheng. Camera-space hand mesh recovery via semantic aggregation and adaptive 2d-1d registration. In *CVPR*, 2021. 1, 2
- [5] F Cini, V Ortenzi, P Corke, and M Controzzi. On the choice of grasp type and location when handing over an object. *Science Robotics*, 2019. 1
- [6] Enric Corona, Albert Pumarola, Guillem Alenya, Francesc Moreno-Noguer, and Grégory Rogez. Ganhand: Predicting human grasp affordances in multi-object scenes. In *CVPR*, 2020. 2, 4
- [7] Jia Deng, Wei Dong, Richard Socher, Li-Jia Li, Kai Li, and Li Fei-Fei. Imagenet: A large-scale hierarchical image database. In *CVPR*, 2009. 7
- [8] Guillermo Garcia-Hernando, Shanxin Yuan, Seungryul Baek, and Tae-Kyun Kim. First-person hand action benchmark with rgb-d videos and 3d hand pose annotations. In *CVPR*, 2018. 1, 2, 6
- [9] Weifeng Ge. Deep metric learning with hierarchical triplet loss. In *ECCV*, 2018. 3
- [10] Kehong Gong, Jianfeng Zhang, and Jiashi Feng. Poseaug: A differentiable pose augmentation framework for 3d human pose estimation. In *CVPR*, 2021. 3
- [11] Patrick Grady, Chengcheng Tang, Christopher D Twigg, Minh Vo, Samarth Brahmabhatt, and Charles C Kemp. Contactopt: Optimizing contact to improve grasps. In *CVPR*, 2021. 2
- [12] Shreyas Hampali, Markus Oberweger, Mahdi Rad, and V. Lepetit. Ho-3d: A multi-user, multi-object dataset for joint 3d hand-object pose estimation. In *arXiv preprint arXiv:1907.01481*, 2019. 8
- [13] Shreyas Hampali, Mahdi Rad, Markus Oberweger, and Vincent Lepetit. Honnotate: A method for 3d annotation of hand and object poses. In *CVPR*, 2020. 1, 2, 6
- [14] Shreyas Hampali, Sayan Deb Sarkar, and Vincent Lepetit. Ho-3d_v3: Improving the accuracy of hand-object annotations of the ho-3d dataset. In *arXiv preprint arXiv:2107.00887*, 2021. 6
- [15] Shreyas Hampali, Sayan Deb Sarkar, Mahdi Rad, and Vincent Lepetit. Handsformer: Keypoint transformer for monocular 3d pose estimation of hands and object in interaction. In *arXiv preprint arXiv:2104.14639*, 2021. 6, 7, 8, 11
- [16] Yana Hasson, Bugra Tekin, Federica Bogo, Ivan Laptev, Marc Pollefeys, and Cordelia Schmid. Leveraging photometric consistency over time for sparsely supervised hand-object reconstruction. In *CVPR*, 2020. 2, 7, 8
- [17] Yana Hasson, Gül Varol, Ivan Laptev, and Cordelia Schmid. Towards unconstrained joint hand-object reconstruction from rgb videos. In *arXiv preprint arXiv:2108.07044*, 2021. 2
- [18] Yana Hasson, Gul Varol, Dimitrios Tzionas, Igor Kalevatykh, Michael J Black, Ivan Laptev, and Cordelia Schmid. Learning joint reconstruction of hands and manipulated objects. In *CVPR*, 2019. 2, 4, 5
- [19] Kaiming He, Xiangyu Zhang, Shaoqing Ren, and Jian Sun. Deep residual learning for image recognition. In *CVPR*, pages 770–778, 2016. 6
- [20] Alexander Hermans, Lucas Beyer, and Bastian Leibe. In defense of the triplet loss for person re-identification. *arXiv preprint arXiv:1703.07737*, 2017. 3
- [21] Tomáš Hodaň, Martin Sundermeyer, Bertram Drost, Yann Labbé, Eric Brachmann, Frank Michel, Carsten Rother, and Jiří Matas. Bop challenge 2020 on 6d object localization. In *ECCV Workshops*, pages 577–594. Springer, 2020. 7
- [22] Hanwen Jiang, Shaowei Liu, Jiashun Wang, and Xiaolong Wang. Hand-object contact consistency reasoning for human grasps generation. In *ICCV*, 2021. 3
- [23] Taeyun Kwon, Bugra Tekin, Jan Stuhmer, Federica Bogo, and Marc Pollefeys. H2o: Two hands manipulating objects for first person interaction recognition. In *ICCV*, 2021. 1
- [24] Jiefeng Li, Chao Xu, Zhicun Chen, Siyuan Bian, Lixin Yang, and Cewu Lu. Hybrik: A hybrid analytical-neural inverse kinematics solution for 3d human pose and shape estimation. In *CVPR*, 2021. 1, 2
- [25] Xiaolong Li, He Wang, Li Yi, Leonidas J Guibas, A Lynn Abbott, and Shuran Song. Category-level articulated object pose estimation. In *CVPR*, 2020. 1
- [26] John Lin, Ying Wu, and Thomas S Huang. Modeling the constraints of human hand motion. In *Proceedings workshop on human motion*, 2000. 4
- [27] Tsung-Yi Lin, Priya Goyal, Ross Girshick, Kaiming He, and Piotr Dollár. Focal loss for dense object detection. In *ICCV*, 2017. 3
- [28] Tsung-Yi Lin, Michael Maire, Serge Belongie, James Hays, Pietro Perona, Deva Ramanan, Piotr Dollár, and C Lawrence Zitnick. Microsoft coco: Common objects in context. In *ECCV*, 2014. 6
- [29] Shaowei Liu, Hanwen Jiang, Jiarui Xu, Sifei Liu, and Xiaolong Wang. Semi-supervised 3d hand-object poses estimation with interactions in time. In *CVPR*, 2021. 2, 7, 8
- [30] Jun Lv, Wenqiang Xu, Lixin Yang, Sucheng Qian, Chongzhao Mao, and Cewu Lu. Handtailor: Towards high-precision monocular 3d hand recovery. In *arXiv preprint arXiv:2102.09244*, 2021. 7
- [31] George Marsaglia et al. Choosing a point from the surface of a sphere. *The Annals of Mathematical Statistics*, 1972. 5
- [32] Matthew Matl. Pyrender. <https://github.com/mmatl/pyrender>, 2019. 6

- [33] A.T. Miller and P.K. Allen. Graspit! a versatile simulator for robotic grasping. *IEEE Robotics Automation Magazine*, 2004. 2
- [34] Franziska Mueller, Florian Bernard, Oleksandr Sotnychenko, Dushyant Mehta, Srinath Sridhar, Dan Casas, and Christian Theobalt. Gnerated hands for real-time 3d hand tracking from monocular rgb. In *CVPR*, 2018. 5
- [35] Neng Qian, Jiayi Wang, Franziska Mueller, Florian Bernard, Vladislav Golyanik, and Christian Theobalt. Hml: A parametric hand texture model for 3d hand reconstruction and personalization. In *ECCV*, 2020. 5
- [36] Javier Romero, Dimitrios Tzionas, and Michael J Black. Embodied hands: Modeling and capturing hands and bodies together. *ToG*, 2017. 3
- [37] Florian Schroff, Dmitry Kalenichenko, and James Philbin. Facenet: A unified embedding for face recognition and clustering. In *CVPR*, 2015. 3
- [38] Abhinav Shrivastava, Abhinav Gupta, and Ross Girshick. Training region-based object detectors with online hard example mining. In *CVPR*, 2016. 3
- [39] Kihyuk Sohn. Improved deep metric learning with multi-class n-pair loss objective. In *NIPS*, 2016. 3
- [40] Xiao Sun, Bin Xiao, Fangyin Wei, Shuang Liang, and Yichen Wei. Integral human pose regression. In *ECCV*, 2018. 2
- [41] Omid Taheri, Nima Ghorbani, Michael J Black, and Dimitrios Tzionas. GRAB: A dataset of whole-body human grasping of objects. In *ECCV*, 2020. 3, 4, 5
- [42] Xiao Tang, Tianyu Wang, and Chi-Wing Fu. Towards accurate alignment in real-time 3d hand-mesh reconstruction. In *ICCV*, 2021. 2
- [43] Bugra Tekin, Federica Bogo, and Marc Pollefeys. H+o: Unified egocentric recognition of 3d hand-object poses and interactions. In *CVPR*, 2019. 6
- [44] Lixin Yang, Jiasen Li, Wenqiang Xu, Yiqun Diao, and Cewu Lu. BiHand: Recovering hand mesh with multi-stage bisected hourglass networks. In *BMVC*, 2020. 2
- [45] Linlin Yang and Angela Yao. Disentangling latent hands for image synthesis and pose estimation. In *CVPR*, 2019. 2
- [46] Lixin Yang, Xinyu Zhan, Kailin Li, Wenqiang Xu, Jiefeng Li, and Cewu Lu. CPF: Learning a contact potential field to model the hand-object interaction. In *ICCV*, 2021. 2, 4, 5
- [47] Yi Zhou, Connelly Barnes, Lu Jingwan, Yang Jimei, and Li Hao. On the continuity of rotation representations in neural networks. In *CVPR*, 2019. 7
- [48] Yuxiao Zhou, Marc Habermann, Weipeng Xu, Ikhsanul Habibie, Christian Theobalt, and Feng Xu. Monocular real-time hand shape and motion capture using multi-modal data. In *CVPR*, 2020. 2
- [49] Christian Zimmermann and Thomas Brox. Learning to estimate 3d hand pose from single rgb images. In *ICCV*, 2017. 5
- [50] Christian Zimmermann, Duygu Ceylan, Jimei Yang, Bryan Russell, Max Argus, and Thomas Brox. Freihand: A dataset for markerless capture of hand pose and shape from single rgb images. In *ICCV*, 2019. 2

Appendix

A. Objects’ Symmetry Axes

In the hand-object interaction dataset, it is far more challenging to predict the pose of an object than in the dataset only contains objects since the objects are often severely occluded by the hand. Therefore, we relax the restrictions of the objects’ symmetry axes similar to [15]. Supposing the set \mathcal{S} contains all the valid rotation matrices based on the object’s predefined symmetry axes, we calculate \mathcal{S} with the following step:

- 1) Firstly, as shown in Fig 8, we align the object to its principal axis of inertia.
- 2) Secondly, we define the axis \mathbf{n} and angle θ of symmetry in Tab 9 under the aligned coordinate system, where the object’s geometry does not change when rotate this object by an angle of θ around \mathbf{n} . Here we get the predefined rotation matrix $\mathbf{R}_{def} = \exp(\theta\mathbf{n})$.
- 3) To get a more accurate rotation matrix \mathbf{R} , we use the Iterative Closest Point (ICP) algorithm to fit a $\Delta\mathbf{R}$. The ICP minimizes the difference between $\Delta\mathbf{R}*\mathbf{R}_{def}*\mathbf{V}_o$ and \mathbf{V}_o , where \mathbf{V}_o is the point clouds on object surface. Finally, we have $\mathbf{R} = \Delta\mathbf{R} * \mathbf{R}_{def}, \mathbf{R} \in \mathcal{S}$.



Figure 8. YCB objects’ principal axis of inertia. The x, y and z axis are colored in red, green and blue, respectively.

B. Additional Results

We demonstrate 20 YCB objects’ MSSD on DexYCB in Tab 10. With ArtiBoost, our network can predict a more accurate pose for almost every object. More qualitative results on HO3D and DexYCB testing set are shown in Fig 9.

| Objects | Axes: \mathbf{n} | Angle: θ |
|-----------------------|--------------------|------------------|
| 002_master_chef_can | x, y, z | 180°, 180°, ∞ |
| 003_cracker_box | x, y, z | 180°, 180°, 180° |
| 004_sugar_box | x, y, z | 180°, 180°, 180° |
| 005_tomato_soup_can | x, y, z | 180°, 180°, ∞ |
| 006_mustard_bottle | z | 180° |
| 007_tuna_fish_can | x, y, z | 180°, 180°, ∞ |
| 008_pudding_box | x, y, z | 180°, 180°, 180° |
| 009_gelatin_box | x, y, z | 180°, 180°, 180° |
| 010_potted_meat_can | x, y, z | 180°, 180°, 180° |
| 024_bowl | z | ∞ |
| 036_wood_block | x, y, z | 180°, 180°, 90° |
| 037_scissors | z | 180° |
| 040_large_marker | x, y, z | 180°, ∞, 180° |
| 052_extra_large_clamp | x | 180° |
| 061_foam_brick | x, y, z | 180°, 90°, 180° |

Table 9. YCB objects’ axes of symmetry used in our experiments. ∞ indicates the object is revolutionary by the axis.

| Objects | Our <i>Clas</i> sym | Our <i>Clas</i> sym + Arti | Objects | Our <i>Clas</i> sym | Our <i>Clas</i> sym + Arti |
|-----------------------|---------------------|-----------------------------------|---------------------|---------------------|-----------------------------------|
| 002_master_chef_can | 27.62 | 25.59 | 003_cracker_box | 63.68 | 46.13 |
| 004_sugar_box | 48.42 | 39.20 | 005_tomato_soup_can | 33.31 | 31.90 |
| 006_mustard_bottle | 35.16 | 32.01 | 007_tuna_fish_can | 24.54 | 23.81 |
| 008_pudding_box | 39.92 | 35.04 | 009_gelatin_box | 45.99 | 37.81 |
| 010_potted_meat_can | 41.44 | 36.47 | 011_banana | 98.69 | 79.87 |
| 019_pitcher_base | 105.66 | 84.82 | 021_bleach_cleanser | 91.66 | 72.31 |
| 024_bowl | 31.74 | 32.37 | 025_mug | 65.46 | 54.28 |
| 035_power_drill | 74.95 | 52.70 | 036_wood_block | 51.24 | 50.69 |
| 037_scissors | 88.10 | 66.52 | 040_large_marker | 30.76 | 29.33 |
| 052_extra_large_clamp | 78.87 | 55.87 | 061_foam_brick | 34.23 | 31.53 |

Table 10. Full MSSD results (*mm*) on **DexYCB** testing set.

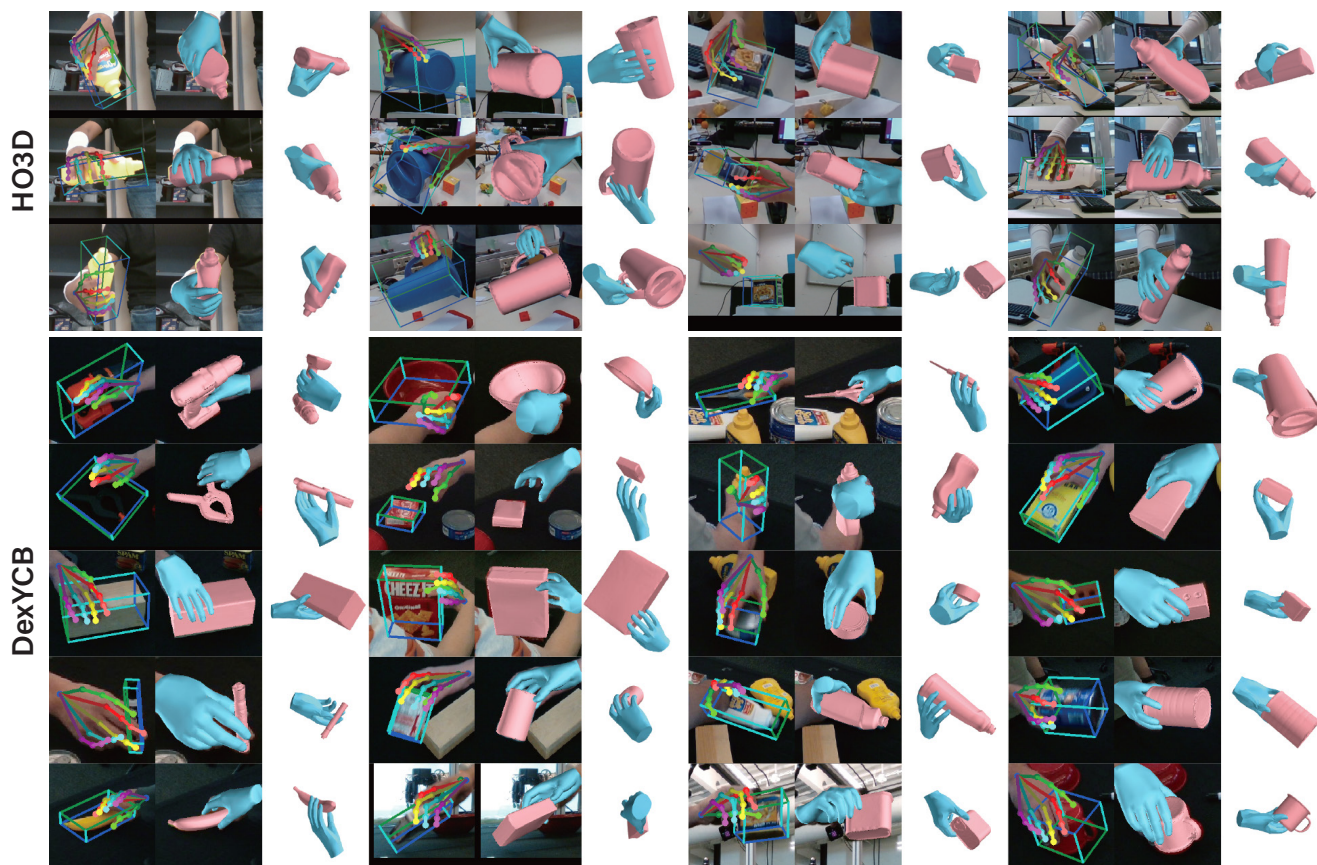


Figure 9. (Best view in color) More qualitative results on **HO3D** (1st ~ 3rd rows) and **DexYCB** (4th ~ 8th rows) datasets.